Hopf bifurcation to square-wave switching in mutually coupled semiconductor lasers

M. Sciamanna,[1,*] M. Virte,[1] C. Masoller,[2] and A. Gavrielides[3]
[1]*Supélec, OPTEL Research Group, Laboratoire Matériaux Optiques, Photonique et Systèmes, EA-4423, 2 rue Edouard Belin, F-57070 Metz, France*
[2]*Departament de Fisica i Enginyeria Nuclear, Universitat Politecnica de Catalunya, Colom 11, E-08222 Terrassa, Barcelona, Spain*
[3]*Air Force Research Laboratory, AFR/EOARD, 86 Blenheim Crescent, Ruislip, Middlesex HA4 7HB, United Kingdom*
(Received 25 May 2012; published 30 July 2012)

Using advanced continuation techniques for dynamical systems, we elucidate the bifurcations leading to asymptotically stable square-wave pulsing and polarization mode switching in semiconductor lasers with mutual time-delayed and polarization rotating coupling. We find that the increase of coupling strength leads to a cascade of Hopf bifurcations on a mixed-mode steady state up to a transcritical bifurcation on a so-called pure-mode steady state where both lasers emit with the injected polarization state. From these successive Hopf bifurcations emerge time-periodic solutions that have a period close to the laser relaxation oscillation for weak coupling but a period close to twice the time delay for large coupling strength. The wave form of the time-periodic solutions also evolves from harmonic pulsing up to square-wave pulsing as has been observed recently in experiments.

DOI: 10.1103/PhysRevE.86.016218 PACS number(s): 05.45.−a, 42.65.Sf, 42.55.Px, 42.60.Mi

I. INTRODUCTION

It is now common knowledge that the dynamics of a semiconductor laser can be modified by the addition of a time-delayed optical feedback (light being reflected back to the laser cavity) [1–4] or a time-delayed optical coupling (unidirectional or mutual coupling from a second laser) [5,6]. When increasing the strength of the time-delayed input, the laser dynamics easily bifurcate from a steady-state to time-periodic, quasiperiodic, or even chaotic pulsating laser output. In most situations the laser dynamics gets a clear spectral signature of the time-delay time scale [7], which can be adjusted by varying the coupling or feedback length. The possibility to generate all-optically pulsating dynamics with a controllable frequency has raised interest towards applications such as optical clock recovery or stable microwave signal generation [8] or, recently, a micro-optical sensing device [9]. On the other hand, chaotic laser outputs have helped to identify new applications of laser diodes in chaos-based cryptography [10] and chaos-based random number generation [11,12].

The wave form of the pulsating laser output is known also to vary as a function of the time delay and nonlinear optical system parameters. This problem was first studied in the case of the so-called Ikeda equation [13] that models a ring nonlinear optical cavities and is of the form $x(t) + T\,dx(t)/dt = \beta f_{\mathrm{NL}}[x(t-\tau)]$. The evolution of a single dynamical variable x is controlled by a first-order filter with time constant T and a time-delayed input with time delay τ and strength β. As shown theoretically and later demonstrated experimentally in a realization using a birefringent plate and optoelectronic feedback [14], the increase of β may lead to a square-wave pulsating dynamics of the x dynamical variable with a period corresponding to 2τ, hence twice the time-delay period. Depending on the ratio between time delay τ and system time scale T, the wave form can vary from square wave to harmonic pulsing [15]. The Hopf bifurcation from which the 2τ pulsating output originates can be sub- or supercritical depending on the form of the nonlinear function f_{NL} [16]. Transition from harmonic pulsing to square-wave pulsing has been studied in more complex and multimode laser systems, including so-called polarization self-modulation in a vertical-cavity surface-emitting laser (VCSEL) with polarization rotating optical feedback [17–20], polarization switching in VCSEL with polarized optical feedback [21], TE-TM mode switching in an edge-emitting laser (EEL) with selective polarization rotating optical feedback [22,23], and more recently in mutually coupled EELs with a polarization rotating scheme [24]. In some configurations square waves are not seen as limit cycle attractors but as slow envelopes of faster chaotic fluctuations such as in chaotic breathers in optoelectronic feedback systems [25] and stairlike chaotic modulation of mutually coupled lasers [26]. Square waves with ultrawide pulse width tunability (from 10 to about 1716 ns) have also been recently reported from polarization switching in a mode-locked fiber laser with high fiber nonlinearity [27].

In this paper, we bring insight into the square-wave switching dynamics as has been observed in mutually coupled EELs with polarization rotating mutual coupling. By increasing the coupling strength, the two lasers exhibit a synchronized square-wave modulation of both TE and TM dynamics. The modal dynamics are anticorrelated, and the square-wave period is twice the time delay of the optical coupling. Although the square-wave dynamics have been numerically well reproduced, their bifurcation origin has never been elucidated. In particular, in Ref. [24], it is mentioned that noise terms in the rate equation model are required to sustain square waves, which otherwise would decay in a transient towards a steady-state dynamics. In contrast, in Ref. [28], asymptotically stable square waves are observed numerically, but the analysis does not capture any Hopf bifurcation with a frequency that relates to the time-delay time scale, in contrast to what is expected in other systems showing square waves. By using here more advanced techniques for bifurcation analysis, we provide evidence that (1) indeed the square-wave dynamics as observed in that system originate from a deterministic bifurcation mechanism, (2) the bifurcation leading to square waves is a cascade of supercritical then subcritical Hopf bifurcations

*marc.sciamanna@supelec.fr

with a limit cycle period increasing from relaxation oscillation period to twice the time-delay period as the coupling strength increases, and (3) the interval of coupling strength where stable deterministic square waves are observed is very small and the stability of these solutions is very marginal, as confirmed by the computation of the Floquet multipliers, and hence can be strongly affected by noise.

Our paper is organized as follows. In Sec. II we summarize for the reader the model and parameters leading to the observation of stable square waves, together with the equations that determine the laser steady states. Section III discusses the stability of the pure-mode steady state and shows that it is determined by a transcritical bifurcation and hence is not associated with the emergence of a stable limit cycle oscillation. In Sec. IV we then apply the continuation techniques to the mixed-mode solution and detail a sequence of Hopf bifurcations to stable square-wave dynamics. We summarize our results in Sec. V.

II. MODEL AND STEADY STATES

In our laser system, two stripe lasers with dominant TE emission are mutually coupled with a selective and polarization rotating time-delayed coupling. More specifically, the outgoing TE field of each laser is rotated to TM emission by a Faraday rotator before being reinjected into the other laser cavity. However, the orientation of the output polarizer of the Faraday rotator ensures that any TM emission from either laser or from secondary reflections would be suppressed in the coupling path. As detailed in Ref. [28], we have modeled the laser system by the following set of equations, which provide square-wave switching in good qualitative agreement with experiments:

$$\frac{dE_{j,x}}{ds} = (1+i\alpha)(g_{j,x}-1)E_{j,x}, \tag{1}$$

$$\frac{dE_{j,y}}{ds} = i\delta E_{j,y} + (1+i\alpha)(g_{j,y}-1-\beta)E_{j,y} + K E_{3-j,x}(s-\theta), \tag{2}$$

$$T\frac{dN_j}{ds} = P - N_j - g_{j,x}I_{j,x} - g_{j,y}I_{j,y}, \tag{3}$$

where $j = 1,2$ denote the two lasers, E_x and E_y are orthogonal linearly polarized slowly varying complex amplitudes (corresponding respectively to TE and TM polarizations), and N is the carrier density. In these equations the time s is normalized by the photon lifetime, i.e., $s = t\kappa$ where κ is the cavity loss rate. $T = \gamma_N/\kappa$ is the ratio between the carrier $(1/\gamma_N)$ and photon $(1/\kappa)$ lifetimes (typically about 1000). δ is the frequency detuning between the x and y polarizations. α is the linewidth enhancement factor. P is the pumping current parameter, normalized such that threshold is obtained for $P = 1$. The parameters of the polarization-orthogonal mutual coupling are K and θ, which represent the normalized coupling strength $K = \eta/\kappa$ and the normalized delay time $\theta = \tau\kappa$, respectively. The modal gains include self- and cross-saturation coefficients:

$$g_{j,x} = N_j/(1+\epsilon_{xx}I_{j,x} + \epsilon_{xy}I_{j,y}), \tag{4}$$

$$g_{j,y} = N_j/(1+\epsilon_{yx}I_{j,x} + \epsilon_{yy}I_{j,y}). \tag{5}$$

The system allows for three steady-state solutions: (a) the mixed-mode solution, in which both lasers emit in x and y polarization simultaneously and which is symmetric upon exchange of both lasers, where $E_{1,x} = E_{2,x} \neq 0$, $E_{1,y} = E_{2,y} \neq 0$, and $N_1 = N_2$, and (b) two pure-mode solutions, in which one laser emits only in the x polarization while the other only emits in the orthogonal polarization, where $E_{1,x} = 0$, $E_{2,x} \neq 0$, $E_{1,y} \neq 0$, $E_{2,y} = 0$ (pure mode 1) or $E_{1,x} \neq 0$, $E_{2,x} = 0$, $E_{1,y} = 0$, $E_{2,y} \neq 0$ (pure mode 2). In essence the laser that emits in the x polarization becomes the master laser which drives the other laser into the orthogonal polarization through the rotated optical injection. The values of the parameters shall be taken from Ref. [28]: $T = 600$ ($\kappa = 300\ \text{ns}^{-1}$ and $\gamma_N = 0.5\ \text{ns}^{-1}$), $\alpha = 3$, $\theta = 900$ (corresponding to a delay time $\tau = 3$ ns), $\beta = 0.04$, $\delta = -0.01$, $\epsilon_{xx} = 0.010$, $\epsilon_{xy} = 0.015$, $\epsilon_{yy} = 0.025$, $\epsilon_{yx} = 0.020$, and $P = 2$.

III. STABILITY ANALYSIS OF THE PURE-MODE STEADY STATE

In this section we shall analyze in more detail the equations determining the steady-state pure mode 1 and its stability. By replacing $E_{j,k} = A_{j,k}e^{i\phi_{j,k}}$ and taking into account the steady-state conditions in Eqs. (1)–(3), we find that the pure mode 1 steady state is determined by

$$I_{2,x} = \frac{P-1}{1+\epsilon_{xx}}, \tag{6}$$

$$\tan\psi = \frac{\delta + \alpha(g_{1,y}-1-\beta)}{g_{1,y}-1-\beta}, \tag{7}$$

$$K^2 = \frac{I_{1,y}}{I_{2,x}}\{[\delta+\alpha(g_{1,y}-1-\beta)]^2 + (g_{1,y}-1-\beta)^2\}, \tag{8}$$

where $I_{j,k} = A_{j,k}^2$ and $\psi = \phi_{2,x} - \phi_{1,y}$. Equation (6) gives the intensity of the master laser (laser 2), which does not depend on the coupling, and Eqs. (7) and (8) allow us to find the intensity of the slave laser (laser 1) as a function of the coupling strength K. The solution is plotted in Fig. 1.

The stability of this pure-mode steady state is determined by a 10×10 evolution matrix from the linearized perturbation equations on the variables $A_{j,k}$, $\phi_{j,k}$, and N_j. However, the selective coupling scheme leads to several submatrices which can be treated separately for the stability analysis.

The equations for the perturbed variables $\delta A_{1,x}$ and $\delta\phi_{1,x}$ read

$$\frac{d\delta A_{1,x}}{ds} = (g_{1,x}-1)\delta A_{1,x}, \tag{9}$$

$$\frac{d\delta\phi_{1,x}}{ds} = \alpha\delta g_{1,x}. \tag{10}$$

Equation (10) gives no information on stability as it is decoupled and depends on the variations of the other quantities. Equation (9) gives the following eigenvalue for stability:

$$\lambda = g_{1,x} - 1 \leqslant 0 \tag{11}$$

or, when combined with the steady-state equations (6)–(8),

$$\epsilon_{xy}(1+\epsilon_{yy})I_{1,y}^{S^2} + [1-(P-1)\epsilon_{yy}+\epsilon_{xy}]I_{1,y}^{S} - (P-1) = 0. \tag{12}$$

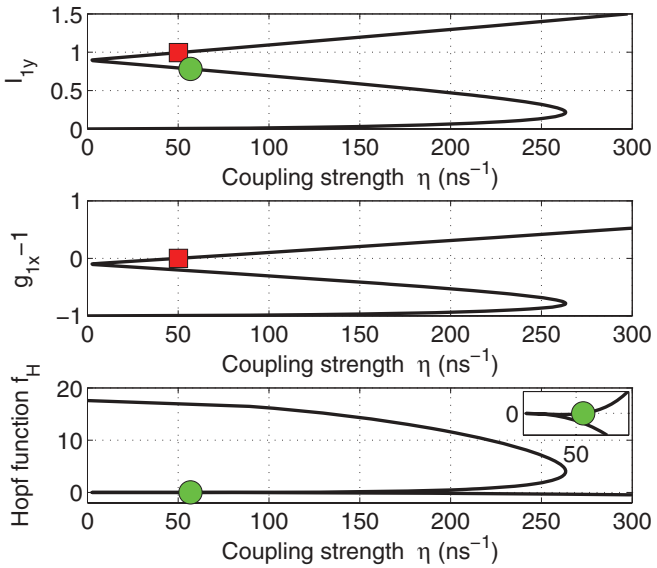

FIG. 1. (Color online) We plot as a function of the coupling strength η (a) the intensity of the I_y polarization of the pure-mode solution, (b) the function determining the transcritical bifurcation $g_{1,y} - 1$, and (c) the function determining the Hopf bifurcation f_H in Eq. (18). The red (dark gray) square in (a) and (b) is for the transcritical bifurcation point. The green (light gray) dot in (a) and (c) is for the Hopf bifurcation.

The pure mode therefore experiences a first bifurcation that is determined by Eq. (12). The bifurcation is transcritical as the eigenvalue is real across the bifurcation point. Equation (12) gives the value of $I_{1,y}$ at the bifurcation point (labeled S), and then Eq. (8) gives the corresponding value of K^S (η^S). Using the same parameters as in Ref. [28], we obtain $K^S = 0.1671$ ($\eta^S = 50.13$ ns^{-1}) and $I^S_{1,y} = 0.9947$ at this bifurcation point. The curve corresponding to Eq. (11) is plotted in Fig. 1, and the transcritical bifurcation is plotted with a red square. On the left of the bifurcation the steady-state pure-mode solution is unstable. The stability of the right-hand part of the branch still has to be examined with the other perturbation equations.

The perturbation equations related to the quantities $\delta A_{2,x}$, $\delta\phi_{2,x}$, and δN_2 form another submatrix that does not depend on the coupling parameters. These equations are similar to the stability analysis of a single-mode laser diode, and one finds two complex conjugate eigenvalues of the form $\lambda = -\xi_2/2 \pm i\omega_2$, where ξ_2 is the damping rate of relaxation oscillations with a frequency ω_2, both including the effect of the gain saturation terms:

$$\xi_2 = \frac{1}{T}\left(1 + \frac{I_{2,x}}{1+\epsilon_{xx}I_{2,x}}\right) + \frac{2\epsilon_{xx}I_{2,x}}{1+\epsilon_{xx}I_{2,x}}, \tag{13}$$

$$\omega_2^2 = \frac{2I_{2,x}}{T}\left(\frac{1+\epsilon_{xx}}{1+\epsilon_{xx}I_{2,x}}\right) - \frac{\xi_2^2}{4}. \tag{14}$$

The eigenvalues have a negative real part and hence correspond to damped nonlinear oscillations of the field and carrier variables. The perturbation equations related to the $\delta A_{2,y}$ and $\delta\phi_{2,y}$ variables do not bring any eigenvalue to the stability analysis. Then only a 3×3 submatrix related to the perturbation equations of the quantities $\delta A_{1,y}$, $\delta\phi_{1,y}$, and δN_1 remains, which is written

$$\frac{d\delta A_{1,y}}{ds} = (g_{1,y} - 1 - \beta - 2N_1 I_{1,y}\epsilon_{yy}m^2)\delta A_{1,y} + mA_{1,y}\delta N_1 + KA_{2,x}\sin(\psi)\delta\phi_{1,y}, \tag{15}$$

$$\frac{d\delta\phi_{1,y}}{ds} = -\left[2\alpha N_1 A_{1,y}m^2\epsilon_{yy} + K\frac{A_{2,x}}{A^2_{1,y}}\sin(\psi)\right]\delta A_{1,y} + \alpha m\delta N_1 - K\frac{A_{2,x}}{A_{1,y}}\cos(\psi)\delta\phi_{1,y}, \tag{16}$$

$$T\frac{d\delta N_1}{ds} = -(1 + mI_{1,y})\delta N_1 - 2A_{1,y}(g_{1,y} - N_1 m^2\epsilon_{yy}I_{1,y})\delta A_{1,y}, \tag{17}$$

where $m = (1 + \epsilon_{yy}I_{1,y})^{-1}$.

An analysis of the stability matrix shows that the condition for the existence of purely imaginary eigenvalues $\lambda_H = i\sigma_H$ (i.e., a Hopf bifurcation point with frequency σ_H) is

$$0 = f_H = (v + \bar{v} - \xi)(v\bar{v} - \xi v - \xi\bar{v} + \bar{u}u + \omega^2) - (v\omega^2 + \alpha u\omega^2 - \xi v\bar{v} - \xi u\bar{u}), \tag{18}$$

where we have defined the following quantities: $v = g_{1,y} - 1 - \beta$, $\bar{v} = v - 2N_1 I_{1,y}m^2\epsilon_{yy}$, $u = \delta + \alpha v$, $\bar{u} = \delta + \alpha\bar{v}$, $\xi = (1 + mI_{1,y})/T$, and $\omega^2 = 2I_{1,y}m^2N_1(1 - m\epsilon_{yy}I_{1,y})/T$.

Equation (18) gives the value of $I_{1,y}$ at the Hopf bifurcation point, and Eq. (8) gives the corresponding value of K_H (η_H). From our choice of parameters we obtain $K_H = 0.1892$ ($\eta_H = 56.77$ ns^{-1}). The corresponding Hopf bifurcation point is plotted with a green dot in Fig. 1.

The frequency of the Hopf bifurcation σ_H is given by the following equation:

$$\sigma_H^2 = v\bar{v} - \xi v - \xi\bar{v} + \bar{u}u + \omega^2 > 0. \tag{19}$$

As can be concluded from Fig. 1 the Hopf bifurcation on the pure-mode steady state is on the unstable part of the pure-mode branch of the solution; hence the emerging time-periodic solution will be initially unstable as well. Moreover, the frequency of the Hopf bifurcation as can be computed from Eq. (19) is close to the relaxation oscillation frequency and hence does not relate to the coupling-induced frequency $1/\tau$ or the frequency of the square-wave solutions $1/2\tau$. There may be more Hopf bifurcations on the pure-mode solution. In particular, keeping the same parameters but decreasing the pump value to $P = 1.5$, we find now three Hopf bifurcations, but all of them are located again on the unstable part of the pure-mode branch. In contrast, increasing the pump value P and with gain saturation coefficients ϵ_{ij} equal to zero, we find now one supercritical Hopf bifurcation located after the transcritical bifurcation that connects to another unstable Hopf point on the pure-mode branch. In this case a stable branch of the time-periodic solution emerges from the pure-mode solution, but the wave form is harmonic and has a frequency again close to the laser relaxation oscillation.

The fact that the pure-mode stability analysis does not bring a pulsation solution at the time-delay period is rather intuitive. As mentioned earlier, the pure-mode solution corresponds to a solution where one of the lasers (the one emitting in x polarization) is the master laser and injects unidirectionally

in the second laser (which for large enough injection switches to y polarization). The pure-mode solution therefore relates to an injection problem with no back (delayed) coupling to the driving laser. This is clear also in the above detailed stability analysis. The delayed terms proportional to $E_{2,x}$ do appear in the 10×10 stability matrix; however, with a few matrix transformations they are eliminated, and the problem reduces to a 3×3 matrix in a block diagonal form. The pure-mode stability is therefore determined by a transcritical bifurcation that does not depend on the delayed coupling parameters.

In summary, although the transcritical bifurcation (or in other parameter ranges, a supercritical Hopf bifurcation) delimits the transition of the laser dynamics to the steady-state polarization of the injected field (pure mode), it does not explain the emergence of the square wave pulsing at twice the time-delay period. We therefore need to investigate then the stability and possible Hopf bifurcations on the mixed-mode steady state.

IV. HOPF BIFURCATIONS ON THE MIXED-MODE STEADY STATE

The steady-state equations determining the mixed-mode steady state have been detailed in Ref. [28]. In contrast to the pure-mode solutions, the stability analysis cannot be performed analytically since one cannot reduce the 10×10 evolution matrix of the perturbation equations to decoupled submatrices. The stability analysis of the mixed-mode solution therefore has to be treated numerically. We have taken advantage of continuation techniques for delay-differential equations (as implemented in the MATLAB package DDE-BIFTOOL) to compute the mixed-mode steady state and its stability as one increases the coupling strength. When detecting a Hopf bifurcation, we are able to compute the emerging branch of stable or even unstable time-periodic solutions and to detect secondary period-doubling or quasiperiodic bifurcations to more complex chaotic dynamics.

The result is plotted in Fig. 2 for the corresponding set of model parameters. The red branch is the branch of the pure-mode steady state (see also Fig. 1). The continuation method finds the same transcritical and Hopf bifurcations as obtained in the analytics of Sec. III. The black branch is the branch of the mixed-mode steady state. As the coupling strength increases, the mixed-mode destabilizes with a first supercritical Hopf bifurcation (for $\eta \sim 37$ ns^{-1}) to a stable branch of time-periodic solutions. However, as will be detailed in the following, this time-periodic solution is a harmonic pulsing at the relaxation oscillation frequency and therefore does not resemble the square-wave pulsing at the 2τ period as seen experimentally and numerically. A further increase of coupling strength leads to a cascade of unstable Hopf bifurcations (unstable because they are on the unstable part of the mixed-mode steady-state branch). Although the emerging time-periodic solutions are initially unstable, they restabilize for larger coupling strength, and one observes therefore the coexistence of several limit cycle attractors with different frequencies in a quite large range of coupling strength values. All the limit cycles emerge from a single steady-state solution. This multistability of time-periodic solutions confirms the observations of many coexisting solutions made numerically

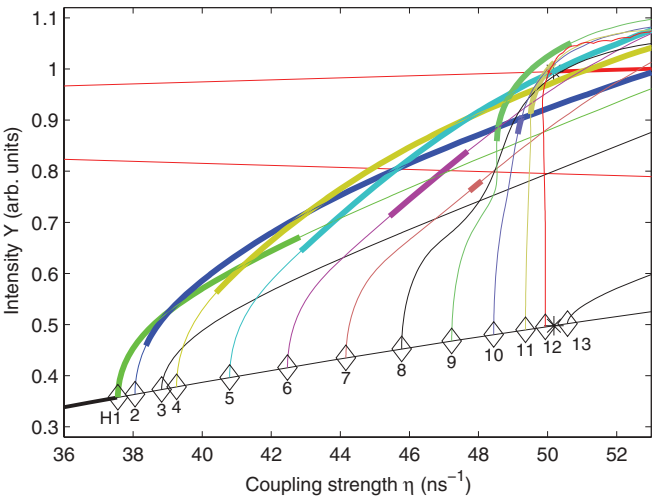

FIG. 2. (Color online) Bifurcation diagram of $I_{y,1}$ as a function of the coupling strength η, as computed using a continuation method. Branches of mixed-mode (black) and pure-mode (red) steady states are plotted together with the Hopf bifurcations labeled H1 to H13 on the mixed-mode steady state. The branches of time-periodic solutions emerging from the different Hopf points are plotted with different colors. The stable parts of the branches of time-periodic solutions are shown in bold. Parameters are defined in the text.

by direct integration of the model rate equations and also observed in experiment [28]. It is interesting to mention that a similar Hopf restabilization mechanism is known in the single feedback laser system, where several limit cycle attractors at frequencies close to the laser relaxation oscillation frequencies (but different by several multiples of the external cavity frequency) can coexist for the same parameters and switching between them occurs randomly in time [29,30]. Again these limit cycles all emerge from a single external cavity mode.

Hopf bifurcation H12, which is the closest one to the transcritical bifurcation point on the pure mode, is different from the other ones because (1) it is subcritical and (2) it restabilizes from a saddle node on the limit cycle to give rise to a stable time-periodic solution in a very narrow range of parameters. As will be confirmed from the analysis of the Hopf bifurcation frequency and from computing the emerging time-periodic wave form, the time-periodic solution emerging from H12 is the square-wave symmetric switching dynamics with 2τ period.

For still larger coupling strength, we detect another Hopf bifurcation, H13, on the mixed-mode solution, but it leads to an unstable time-periodic solution at a frequency close to the relaxation oscillation frequency (see also Fig. 3). The H13 Hopf bifurcation is located after the transcritical bifurcation that leads to a stable pure-mode solution; hence the laser system in that coupling range is inevitably attracted to the stable steady-state pure-mode solution.

To gain insight into the emerging time-periodic solutions, we plot in Fig. 3 the period of the laser pulsing along the different branches of time-periodic solutions as a function of the coupling strength η. The two dashed lines indicate the time-delay value ($\tau = 3$ ns) and the value as expected for the square-wave pulsing dynamics 2τ. One can therefore

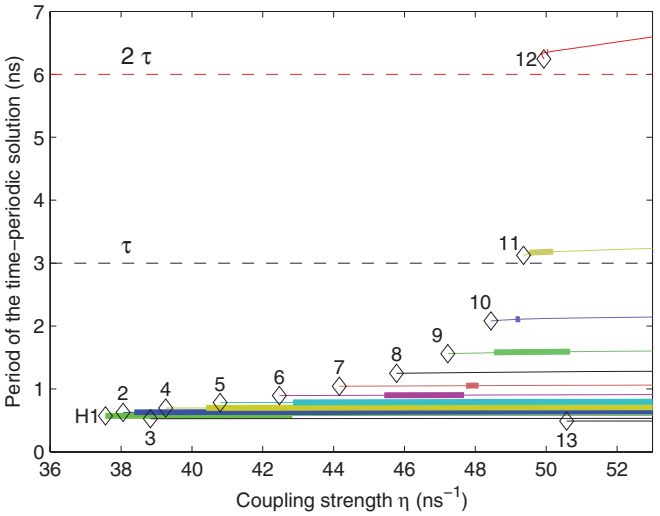

FIG. 3. (Color online) Period of the time-periodic solutions along the different branches shown in Fig. 2 and emerging from the Hopf points labeled H1 to H13. The stable parts of the branches of time-periodic solutions are shown in bold. The dashed lines indicate a time period equal to τ or 2τ, where τ is the time delay in the laser mutual coupling.

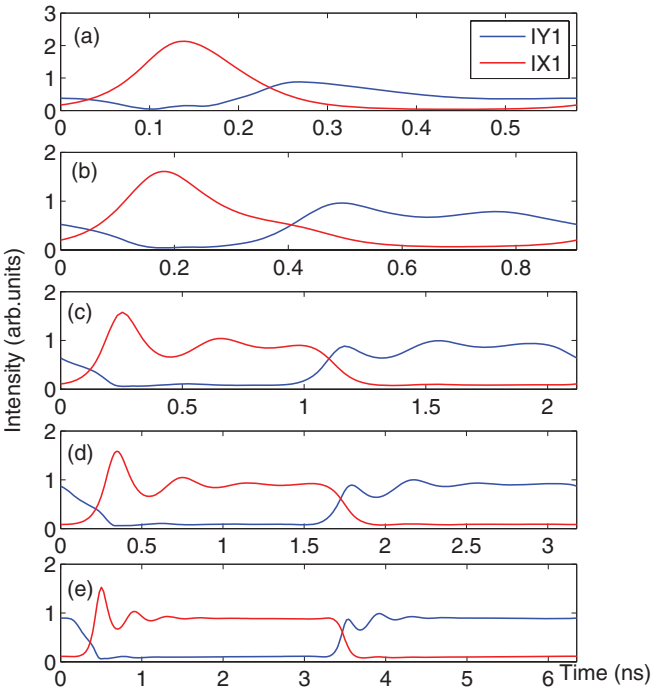

FIG. 4. (Color online) Samples of the time-periodic pulsing computed along the different branches of time-periodic dynamics in Fig. 2. Only the x-mode [red (light gray)] and y-mode [blue (dark gray)] intensities of laser 1 are plotted, but the solutions are the same for laser 2. (a) Branch 1, $\eta = 49.98$ ns^{-1}, (b) branch 6, $\eta = 50.14$ ns^{-1}, (c) branch 10, $\eta = 49.95$ ns^{-1}, (d) branch 11, $\eta = 50.02$ ns^{-1}, and (e) branch 12, $\eta = 50.00$ ns^{-1}. Branch j means that it emerges from the Hopf bifurcation labeled j in Fig. 2.

immediately compare the period of the laser pulsing, as computed by the continuation method, and the system and coupling delay time scales. The first Hopf bifurcation H1 has a period of about 0.5 ns, which is close to the laser relaxation oscillation period. The Hopf frequency decreases, hence the period of the pulsing dynamics increases, as one increases the coupling strength. Hopf bifurcation H11 leads to time-periodic dynamics at a period close to the time-delay value $\tau = 3$ ns. Hopf bifurcation H12 finally leads to a time-periodic pulsing with a period of about $2\tau = 6$ ns; hence it is a good candidate to generate the 2τ square-wave forms we observe numerically and experimentally. Hopf bifurcation H13 yields again a time-periodic solution with a period close to the relaxation oscillation period.

To further analyze the time-periodic dynamics emerging from the mixed-mode Hopf points, we plot in Fig. 4 the computed wave forms along the different branches of time-periodic solutions that appear successively when increasing the coupling strength. All the subplots correspond to a single period of the time-periodic dynamics. The dynamics is the same in both lasers and is here only shown for laser 1. In all cases in Figs. 4(a)–4(e) the intensities of the x- and y-polarization modes are anticorrelated. The case in Fig. 4(a) corresponds to a harmonic pulsing with a period of about 0.58 ns, which is close to the relaxation oscillation period of the free-running lasers for this operating current. Such a harmonic pulsing emerges from the first supercritical Hopf (H1) point on the mixed-mode branch. As one increases the coupling strength, the system experiences a cascade of Hopf bifurcations to different limit cycle attractors with different frequencies, as demonstrated in Fig. 3. This is further confirmed in Fig. 4, which shows that the time period of the pulsing dynamics ranges from about the relaxation oscillation period in Fig. 4(a) to a slightly longer period in Figs. 4(b) and 4(c) up to the time-delay value in Fig. 4(d) and twice the time-delay value in Fig. 4(e). The wave form also changes when one looks at the different limit cycle dynamics. The wave forms of the time-periodic dynamics emerging from the first Hopf point, H1 [Fig. 4(a)], is a harmonic pulsing with single pulses at the relaxation oscillation period, which complexifies into a squarelike wave form made of damped relaxation oscillations modulated by a slower time period in Fig. 4(c). The wave forms emerging from the H11 and H12 bifurcation points are square-wave forms at either the time-delay value or twice the time-delay value.

All these different wave forms in Figs. 4(a)–4(e) with different time periods are stable in a given range of the coupling strength, and the continuation method also unveils the coexistence of several of these limit cycle attractors for the same value of the coupling strength. One identifies here a clear interest of the continuation technique, which is able to follow time-periodic dynamics irrespective of their stability. A direct numerical integration would only identify the stable attractors, and to find coexisting solutions we need a very careful mapping of the dynamics by varying the initial conditions and/or forcing numerically jumps between the coexisting solutions. The square-wave forms in Figs. 4(c) and 4(d) have not been found in the numerics of Ref. [28] or in the experiment of Ref. [24], but our continuation method confirms they correspond to stable attractors in a given range of the coupling strength. We have then complemented our simulations of Ref. [28] by looking more systematically for square-wave time-periodic dynamics

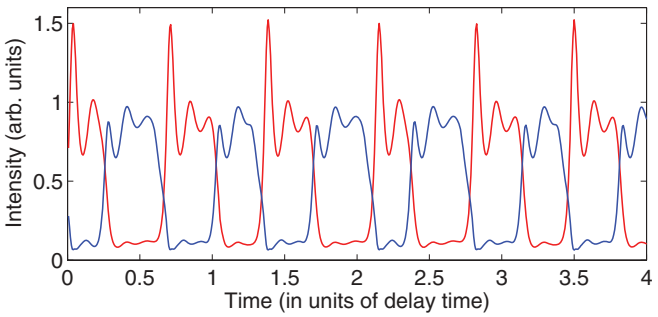

FIG. 5. (Color online) Square-wave switching with a period close to the delay time τ, obtained by direct integration of the rate equations. The coupling strength is $\eta = 49.60\ \mathrm{ns}^{-1}$. Only the x-mode [red (light gray)] and y-mode [blue (dark gray)] intensities of laser 1 are plotted, but the solutions are the same for laser 2.

with a period close to τ. Figure 5 shows one such case obtained numerically by direct integration of the rate equations, where the square-wave dynamics has a period close to τ, resembling the one obtained by continuation in Fig. 4(c).

The square-wave form in Fig. 4(e) agrees with the one found numerically and experimentally, but such a solution emerges from an unstable (subcritical) Hopf bifurcation which cannot be detected simply by numerical integration. As shown in Fig. 6, we furthermore observe that as the time-periodic solution along the branch emerging from H12 destabilizes, the square-wave form also changes its shape while keeping the same time period equal to 2τ. The stable 2τ square-wave form has both x- and y-mode intensities above zero [Fig. 6(a)], while the unstable 2τ square-wave form has both polarization mode intensities reaching zero as time increases. This feature has been observed numerically in the transient square-wave dynamics towards the pure-mode steady state in Ref. [28] and now receives theoretical confirmation from the stability analysis of the time-periodic solutions.

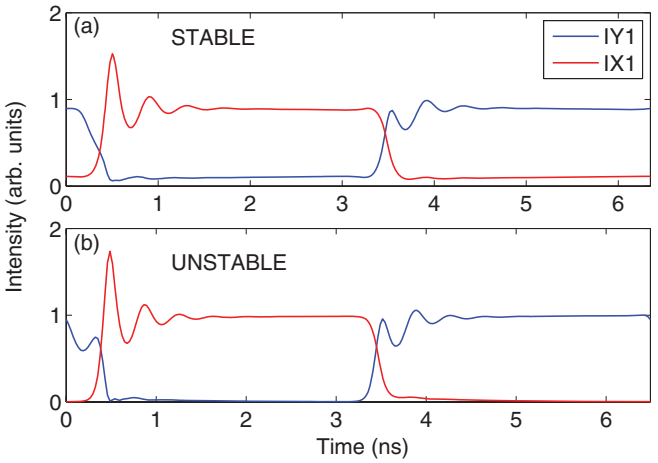

FIG. 6. (Color online) Comparison between stable and unstable square-wave dynamics at the 2τ period, along the branch emerging from Hopf bifurcation H12. (a) Stable solution, $\eta = 50.00\ \mathrm{ns}^{-1}$ and (b) unstable solution, $\eta = 51.74\ \mathrm{ns}^{-1}$. Only the x-mode [red (light gray)] and y-mode [blue (dark gray)] intensities of laser 1 are plotted, but the solutions are the same for laser 2.

The combination of Figs. 2–4 provides a deterministic explanation for the square-wave switching in this laser system. As one increases the coupling strength, the laser experiences a cascade of first supercritical Hopf bifurcation at the relaxation oscillation frequency and then successively unstable Hopf bifurcations to limit cycle attractors of different frequencies and different wave forms. These wave forms can restabilize through an increase of the coupling strength. For a large enough coupling strength and as the system approaches the transcritical bifurcation to pure-mode steady-state, square-wave time-periodic dynamics emerges from Hopf bifurcations with a frequency that relates to the inverse of the coupling delay time.

V. CONCLUSIONS

In summary, we have provided a deterministic bifurcation explanation for the square-wave switching dynamics in a laser system made of two mutually coupled edge-emitting lasers with polarization rotating time-delayed coupling. As the coupling strength increases, the laser exhibits a cascade of Hopf bifurcations to time-periodic dynamics with different frequencies and different wave forms. For small coupling the Hopf bifurcation is supercritical, and the time-periodic dynamics is a harmonic wave form with a period close to the relaxation oscillation period. For larger coupling and before a transition (transcritical bifurcation) to a steady-state dynamics, the laser undergoes a Hopf bifurcation to square-wave dynamics with a period equal to the time delay τ or to twice the time-delay value, 2τ. Square-wave forms where the mode intensity reaches zero are found to be unstable. The laser shows coexistence of several limit cycle attractors with therefore different wave forms and frequencies in a large range of the coupling strength. These results are made possible thanks to the use of advanced continuation techniques that allow us to track time-periodic solutions irrespective of their stability, in contrast to conventional direct integration of the rate equations. Combined with the analytics on the Hopf bifurcation for the so-called pure-mode steady state, this work sheds light on both our previous numerical studies and the experimental observations. In particular, it would be interesting to find a square wave of period τ also in experiment since this is shown here to be a coexisting stable limit cycle attractor. Finally, this work demonstrates that square-wave dynamics is a stable attractor in this laser system and does not need or is not supported by the addition of noise. This result is the consequence of the additional complexity of our model equations (1)–(3) with respect to the equations of Ref. [24]. The inclusion of gain saturation coefficients and frequency detuning has made it possible to identify a relatively small range of coupling strengths where square-wave time-periodic switching dynamics is an asymptotically stable solution. In the model of Ref. [24], without these additional terms only transient square-wave dynamics were found. How much the asymptotic stability of square-wave dynamics depends on the gain saturation and detuning values remains an interesting question for future work but requires an in-depth continuation of bifurcations in a multiparameter space. Experimentally, it is not possible to conclude from the time traces of Ref. [24] whether the observed square-wave dynamics is an unstable,

but noise-sustained, transient dynamics or a deterministic asymptotically stable square-wave switching of the kind shown in Fig. 6. Indeed time traces are recorded on a short time span, and a careful tracking of the transition from stable to unstable square waves would require a very fine tuning of the coupling strength.

ACKNOWLEDGMENTS

This research was supported by the Interuniversity Attraction Poles program of the Belgian Science Policy Office under Grant No. IAP P7-35 "photonics@be," the Conseil Regional de Lorraine, and Fondation Supelec.

[1] A. Hohl and A. Gavrielides, Phys. Rev. Lett. **82**, 1148 (1999).
[2] R. Lang and K. Kobayashi, IEEE J. Quantum Electron. **16**, 347 (1980).
[3] R. W. Tkach and A. R. Chraplyvy, IEEE J. Lightwave Technol. **4**, 1665 (1986).
[4] T. Sano, Phys. Rev. A **50**, 2719 (1994).
[5] H.-J. Wünsche, S. Bauer, J. Kreissl, O. Ushakov, N. Korneyev, F. Henneberger, E. Wille, H. Erzgräber, M. Peil, W. Elsäßer, and I. Fischer, Phys. Rev. Lett. **94**, 163901 (2005).
[6] C. Bonatto, B. Kelleher, G. Huyet, and S. P. Hegarty, Phys. Rev. E **85**, 026205 (2012).
[7] D. Rontani, A. Locquet, M. Sciamanna, and D. S. Citrin, Opt. Lett. **32**, 2960 (2007).
[8] B. Sartorius, C. Bornholdt, O. Brox, H. Ehrke, D. Hoffmann, R. Ludwig, and M. Mohrle, Electron. Lett. **34**, 1664 (1998).
[9] S. Ura, S. Shoda, K. Nishio, and Y. Awatsuji, Opt. Express **19**, 23683 (2011).
[10] C. Mirasso, P. Colet, and P. Garcia-Fernandez, IEEE Photonics Technol. Lett. **8**, 299 (1996).
[11] A. Uchida, K. Amano, M. Inoue, K. Hirano, S. Naito, H. Someya, I. Oowada, T. Kurashige, M. Shiki, S. Yoshimori, K. Yoshimura, and P. Davis, Nat. Photonics **2**, 728 (2008).
[12] I. Kanter, Y. Aviad, I. Reidler, E. Cohen, and M. Rosenbluh, Nat. Photonics **4**, 58 (2010).
[13] K. Ikeda, Opt. Commun. **30**, 257 (1979).
[14] L. Larger, J.-P. Goedgebuer, and J.-M. Merolla, IEEE J. Quantum Electron. **34**, 594 (1998).
[15] T. Erneux, L. Larger, M. W. Lee, and J.-P. Goedgebuer, Phys. D **194**, 49 (2004).
[16] L. Larger, J.-P. Goedgebuer, and T. Erneux, Phys. Rev. E **69**, 036210 (2004).
[17] S. Jiang, Z. Pan, M. Dagenais, R. A. Morgan, and K. Kojima, Appl. Phys. Lett. **63**, 3545 (1993).
[18] H. Li, A. Hohl, A. Gavrielides, H. Hou, and K. D. Choquette, Appl. Phys. Lett. **72**, 2355 (1998).
[19] M. Sciamanna, F. Rogister, O. Deparis, P. Mégret, M. Blondel, and T. Erneux, Opt. Lett. **27**, 261 (2002).
[20] M. Sciamanna, T. Erneux, F. Rogister, O. Deparis, P. Mégret, and M. Blondel, Phys. Rev. A **65**, 041801 (2002).
[21] P. Besnard, F. Robert, M. L. Charès, and G. M. Stéphan, Phys. Rev. A **56**, 3191 (1997).
[22] A. Gavrielides, T. Erneux, D. W. Sukow, G. Burner, T. McLachlan, J. Miller, and J. Amonette, Opt. Lett. **31**, 2006 (2006).
[23] A. Gavrielides, D. W. Sukow, G. Burner, T. McLachlan, J. Miller, and J. Amonette, Phys. Rev. E **81**, 056209 (2010).
[24] D. W. Sukow, A. Gavrielides, T. Erneux, B. Mooneyham, K. Lee, J. McKay, and J. Davis, Phys. Rev. E **81**, 025206 (2010).
[25] Y. C. Kouomou, P. Colet, L. Larger, and N. Gastaud, Phys. Rev. Lett. **95**, 203903 (2005).
[26] E. A. Viktorov, A. M. Yacomotti, and P. Mandel, J. Opt. B **6**, L9 (2004).
[27] X. Zhang, C. Gu, G. Chen, B. Sun, L. Xu, A. Wang, and H. Ming, Opt. Lett. **37**, 1334 (2012).
[28] C. Masoller, D. Sukow, A. Gavrielides, and M. Sciamanna, Phys. Rev. A **84**, 023838 (2011).
[29] J. Mork, B. Tromborg, and J. Mark, IEEE J. Quantum Electron. **28**, 93 (1992).
[30] A. Ritter and H. Haug, IEEE J. Quantum Electron. **29**, 1064 (1993).